J. Fluid Mech. (1982), *vol.* 125, *pp.* 411–427
Printed in Great Britain

Three-dimensional stability of vortex arrays

By A. C. ROBINSON AND P. G. SAFFMAN
Applied Mathematics, California Institute of Technology, Pasadena, California 91125

(Received 18 January 1982 and in revised form 1 June 1982)

The stability to three-dimensional disturbances of three classical steady vortex configurations in an incompressible inviscid fluid is studied in the limit of small vortex cross-sectional area and long axial disturbance wavelength. The configurations examined are the single infinite vortex row, the Kármán vortex street of staggered vortices and the symmetric vortex street. It is shown that the single row is most unstable to a two-dimensional disturbance, while the Kármán vortex street is most unstable to a three-dimensional disturbance over a significant range of street spacing ratios. The symmetric vortex street is found to be most unstable to three-dimensional or two-dimensional symmetric disturbances depending on the spacing ratio of the street. Short remarks are made concerning the relevance of the calculations to the observed instabilities in free shear layer, wake and boundary-layer type flows.

1. Introduction

The linear stability to two-dimensional disturbances of a single infinite row of corotating line vortices and of the symmetric and staggered double rows of contra-rotating vortices in a perfect fluid was first treated by Kármán (1911, 1912) and Kármán & Rubach (1912). Lamb (1932) gives a careful exposition of much of the analysis. It is found that all configurations are unstable to infinitesimal two-dimensional disturbances except for a single configuration of the staggered vortex street in which the street spacing ratio (the distance between the rows divided by the separation of vortices in the same row) is 0·281. In particular, the staggered street, known as the Kármán vortex street, has attracted much attention (Rosenhead 1953; Wille 1960). The observations of coherent structures in the turbulent mixing layer has stimulated during the last decade much study of the single infinite row.

The subject of vortex interaction and stability is currently of great interest and the correct interpretation of vortex stability calculations with respect to experimental data is uncertain (Saffman 1981). An understanding of the linear stability of the above-mentioned vortex configurations in an inviscid fluid to not only two-dimensional disturbances but also three-dimensional disturbances, including the effects of significant finite vortex cross-sectional area, would be of much value in interpreting the observed phenomena in real flows, and we propose in this paper to document quantitative results for the three-dimensional linear stability of the single row of vortices, the Kármán vortex street and the symmetric double row of vortices. The results will be limited, however, in the present work to the case of large vortex separation and long-axial-wavelength disturbances where the distance between the vortices and the wavelength of the three-dimensional motion is referred to the radius of the cores. The evolution of the arrays to three-dimensional disturbances of arbitrary size can then be analysed using the Biot–Savart law to compute the induced motion of the vortices and the cutoff approximation to compute the self-induced

velocity of the individual vortices. The behaviour of infinitesimal disturbances is obtained by linearizing the equations of motions about the steady state and then Fourier analysing in both the vortex axial direction and the row direction to reduce the linear stability equations to a finite system. The configuration is unstable to disturbances of a given axial and row wavelength if there exist exponentially growing solutions, and stable (that is, neutrally stable) if there exist only oscillatory solutions to the reduced system. It should be noted that the wavelength in the row direction need not be an integral multiple of the vortex separation, which is the spatial period of the undisturbed array.

Schlayer (1928) and Rosenhead (1930) have discussed the stability of the Kármán vortex street to three-dimensional disturbances in this limit. Schlayer formulates the problem completely, but only gives qualitative results. Rosenhead's treatment is incomplete as it neglects the influence of transverse disturbance wavelength except for the stabilizing effect of the self-induction of a single vortex. Also, both authors introduce the cutoff approximation as an *ad hoc* assumption (there is, incidentally, no discussion of three-dimensional vortex stability in Lamb (1932)). Moreover, the complexity of the algebraic expressions and the labour required to evaluate them by hand limited the results to a few cases. One of our purposes here is to give further data for this flow. Formally consistent asymptotic expansions have now been given to justify the cutoff approximation and find the higher-order corrections (Moore & Saffman 1972) and the stability to three-dimensional disturbances of several other vortex configurations have been documented in the literature. Widnall (1975) and Saffman & Baker (1979) have reviewed much of this work. In addition to the work of Schlayer and Rosenhead on rectilinear vortex configurations, Gopal (1963) and Crow (1970) studied the case of a pair of contrarotating vortices, and Jimenez (1975) examined the corotating pair.

Although the effects of finite area are beyond the scope of the present work, it is perhaps appropriate to mention what has been achieved in this connection. With regards to the effect of vortex separations comparable to the size of the vortices, Saffman & Szeto (1981) have shown there is little effect on the two-dimensional stability of a single row. On the other hand Christiansen & Zabusky (1973) give suggestive numerical evidence and Saffman & Schatzman (1982*a*) show from linear stability calculations that giving the vortices finite area in a Kármán vortex street can stabilize the vortices to two-dimensional disturbances.

For disturbances with axial wavelength comparable to the diameter of the vortex it has been shown that a rectilinear vortex may become unstable (Widnall, Bliss & Tsai 1974; Widnall 1975; Moore & Saffman 1975). This parametric instability may occur when the vortex is subject to a straining field if it happens that the frequencies of two normal modes coincide in such a way as to allow a standing wave to occur; the external field may then cause the vortex to become unstable. A similar instability is allowed by the cutoff theory outside its range of validity, and, although we shall at times show this instability in subsequent stability diagrams, it is to be understood that the axial wavenumber, width and magnitude of the instability are to be taken *only in a qualitative sense* as an indication of the phenomena, as the instability may or may not be real depending on the internal structure of the vortex filament. A case where the cutoff prediction is spurious is given by Moore & Saffman (1974).

Pierrehumbert (1980) (see also Pierrehumbert & Widnall 1982) has examined the stability to three-dimensional disturbances of the Stuart (1967) solution of the Euler equations, which describes a single infinite row of continuous vortices, the flow varying from a hyperbolic-tangent shear-layer profile to a single infinite row of point

vortices according to the value of a single parameter. Two types of disturbances are considered, one in which all the vortices are deformed in exactly the same manner and one in which the wavelength of the disturbance in the row direction is twice the separation, and neighbouring vortices move in an antisymmetrical way. The former gives rise to the short-axial-wavelength parametric instability, which cannot be calculated properly by the Biot–Savart induction law. The latter agrees reasonably in the long-wavelength limit with the calculations of the present work.

Our calculations of the long-wavelength instability of well-separated vortex arrays are restricted to the cooperative modes of instability, which depend primarily on the mutual induction. It is expected that the results will, however, be at least qualitatively informative for arrays containing vortices of significant area and determine when two-dimensional or three-dimensional disturbances are likely to be the more important. Also, the parametric dependence of stability characteristics relative to arbitrary row-wise wavelength is easily determined; that is, there is no restriction on the allowed subharmonic disturbance. The mathematical formulation of the problem is given in §2. The results for the single row are described in §3, the results for the Kármán vortex street are contained in §4, and §5 describes the case of the symmetrical double row. A summary and comparison of the three cases is given in §6.

2. Analysis

Our analysis, which leads up to a finite-dimensional eigenvalue problem, follows in the spirit of the previous work of Crow (1970) and Lamb (1932). We give details for the symmetric double row since the results for the single row and staggered double row follow immediately. The symmetric double row consists of two straight rows of vortices with the axis of each vortex aligned with the **k**- or z-direction. The rows are aligned in the **i**- or x-direction. The first row is assumed to lie in the plane $y = 0$, with each vortex having circulation Γ. The second row lies in the plane $y = -h$, with each vortex having circulation $-\Gamma$. The vortices in each row are separated by a distance l. See figure 1 for a sketch of all configurations. A parametric representation of the position of each element of each vortex filament is given by

$$\mathbf{R}_m = (ml + Ut + x_m(\rho_m, t))\,\mathbf{i} + y_m(\rho_m, t)\,\mathbf{j} + (\rho_m + z_m(\rho_m, t))\,\mathbf{k}, \tag{2.1}$$

$$\mathbf{R}_n = (nl + Ut + x_n(\rho_n, t))\,\mathbf{i} + (-h + y_n(\rho_n, t))\,\mathbf{j} + (\rho_n + z_n(\rho_n, t))\,\mathbf{k}, \tag{2.2}$$

where the subscript m denotes a vortex on the first row and n a vortex on the second row and these subscripts range over all integral values. The Lagrangian variable ρ takes on values in $-\infty < \rho < +\infty$. U denotes the induced velocity of the undisturbed vortex street. For a vortex m on the first row the velocity field is given by

$$\mathbf{U}_m(\mathbf{R}_m) = \sum_p \frac{\Gamma}{4\pi} \int_{[c]_{p-m}} \frac{(\mathbf{R}'_p - \mathbf{R}_m) \wedge d\mathbf{R}'_p}{|\mathbf{R}'_p - \mathbf{R}_m|^3} - \sum_q \frac{\Gamma}{4\pi} \int \frac{(\mathbf{R}'_q - \mathbf{R}_m) \wedge d\mathbf{R}'_q}{|\mathbf{R}'_q - \mathbf{R}_m|^3}, \tag{2.3}$$

where the summation is over all integral values of p and q. We take as a convention that summation in the dummy variable p refers to contributions from vortices on the first row, and for contributions from the second row we sum in the variable q. The symbol $[c]_{p-m}$ indicates that a cutoff length c is implemented on each side of the singularity in the integrand for $p = m$. The equations of motion are then

$$\frac{\partial x_m}{\partial t} + U = u_m, \quad \frac{\partial y_m}{\partial t} = v_m, \quad \frac{\partial z_m}{\partial t} = w_m, \tag{2.4}$$

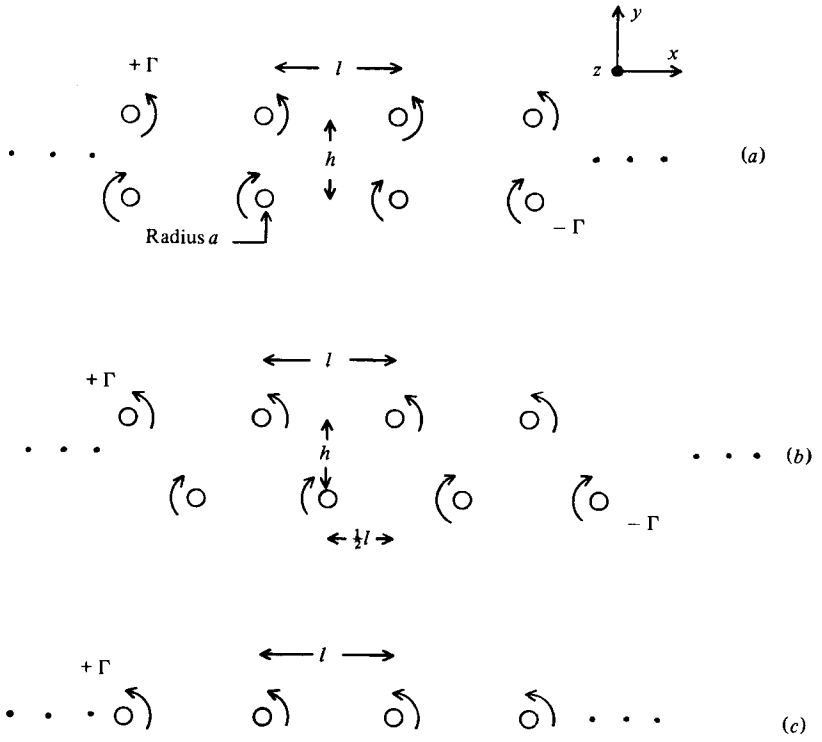

FIGURE 1. Steady vortex configurations (two-dimensional (x, y)-plane cross-section): (*a*) symmetric double row; (*b*) staggered double row or Kármán vortex street; (*c*) single row.

where $\mathbf{U}_m(\mathbf{R}_m) = u_m\mathbf{i} + v_m\mathbf{j} + w_m\mathbf{k}$. For points on the lower row similar equations are obtained. The equations are linearized to first order in $\partial x/\partial\rho$, x/l, x/h for all x on both the first and second rows, and similarly for each y and z. Upon doing this, zeroth-order terms are satisfied identically. An infinite-dimensional autonomous linear system in x_m, y_m and z_m, and x_n, y_n and z_n results. Now setting

$$\left.\begin{aligned} x_m &= \hat{x}_m e^{ik\rho_m}, \quad y_m = \hat{y}_m e^{ik\rho_m}, \quad z_m = \hat{z}_m e^{ik\rho_m}, \\ x_n &= \hat{x}_n e^{ik\rho_n}, \quad y_n = \hat{y}_n e^{ik\rho_n}, \quad z_n = \hat{z}_n e^{ik\rho_n}, \end{aligned}\right\} \tag{2.5}$$

we specify a sinusoidal disturbance of wavenumber $k = 2\pi/\lambda$ in the axial or spanwise direction at each vortex position on both the first and second rows. A general disturbance could be represented by a Fourier superposition of solutions. The analysis is somewhat involved but straightforward, and the following equations for points on the first row are obtained:

$$\begin{aligned} \frac{\partial\hat{x}_m}{\partial t} = &-\frac{\Gamma}{2\pi}\sum_p{}' \frac{\hat{y}_m - \psi_p\hat{y}_p}{l_{pm}^2} + \frac{\Gamma}{2\pi}k^2\omega(kc)\,\hat{y}_m \\ &+ \frac{\Gamma}{2\pi}\sum_q \frac{(l_{qm}^2 - h^2)\,\hat{y}_m - (l_{qm}^2\,\psi_q - h^2\chi_q)\,\hat{y}_q}{L_{qm}^4} \\ &+ \frac{\Gamma}{2\pi}\sum_q \frac{l_{qm}h(2\hat{x}_m - (\chi_q + \psi_q)\,\hat{x}_q)}{L_{qm}^4}, \end{aligned} \tag{2.6}$$

$$\frac{\partial \hat{y}_m}{\partial t} = -\frac{\Gamma}{2\pi}\sum_p{}' \frac{\hat{x}_m - \chi_p \hat{x}_p}{l_{pm}^2} - \frac{\Gamma}{2\pi} k^2 \omega(kc)\, \hat{x}_m$$
$$+ \frac{\Gamma}{2\pi}\sum_q \frac{(l_{qm}^2 - h^2)\,\hat{x}_m - (l_{qm}^2 \chi_q - h^2 \psi_q)\,\hat{x}_q}{L_{qm}^4}$$
$$- \frac{\Gamma}{2\pi}\sum_q \frac{l_{qm} h (2\hat{y}_m - (\chi_q + \psi_q)\,\hat{y}_q)}{L_{qm}^4}, \tag{2.7}$$

$$\frac{\partial \hat{z}_m}{\partial t} = -\frac{\Gamma}{2\pi}\sum_q \frac{ihk}{L_{qm}^2}\chi_q \hat{x}_q, \tag{2.8}$$

where

$$\chi(\xi) = \xi K_1(\xi), \quad \psi(\xi) = \xi^2 K_0(\xi) + \xi K_1(\xi), \tag{2.9a, b}$$

$$\omega(\xi) = \frac{1}{2}\left[\frac{\cos\xi - 1}{\xi^2} + \frac{\sin\xi}{\xi} - \mathrm{Ci}\,(\xi)\right]. \tag{2.9c}$$

The functions χ and ψ are Crow's first and second mutual-induction functions respectively and ω is his self-induction function. K_0, K_1 and Ci are modified Bessel functions of the second kind and the integral cosine function respectively. It is easily shown that both χ and ψ have a value of 1·0 at $\xi = 0{\cdot}0$. The functions go to zero exponentially for large arguments and are essentially negligible for ξ greater than 5·0. The axial wavenumber k is assumed from henceforth to be non-negative to avoid constant repetition of absolute-value signs. The subscripts on ψ and χ indicate that the function arguments are $|l_{pm}|\,k$ and $L_{qm}k$ for subscripts p and q respectively, where $l_{pm} = (p-m)\,l$ and $L_{qm}^2 = l_{qm}^2 + h^2$, with $l_{qm} = (q-m)\,l$. The equations have been put into a form such that in the limit $k \to 0$ the stability equations of Lamb for the two-dimensional case are obtained.

The cutoff length c is chosen from the formula (Moore & Saffman 1972)

$$c = \tfrac{1}{2} a e^{\frac{1}{4}} f, \quad f = \exp\left(\tfrac{1}{4} - \frac{4\pi^2}{\Gamma^2}\int_0^a v^2 a'\,da'\right), \tag{2.10}$$

where v represents the distribution of swirl velocity in the core and we have assumed no axial velocity in the core. For uniform vorticity $f = 1$, and all results presented in this paper have assumed $f = 1$. Since the asymptotic theory using the cutoff method is accurate only to $O(ka)^2$, the function ω is replaced by the leading-order terms giving

$$\omega(kc) \approx \frac{1}{2}\left[\ln\frac{2}{kaf} - \gamma + \tfrac{1}{4}\right] = \theta(ka), \tag{2.11}$$

where $\gamma = 0{\cdot}5772\ldots$ is Euler's constant.

It may now be noted that the $\hat{x}$- and $\hat{y}$-equations decouple from the $\hat{z}$-equations and that for considerations of stability it is sufficient to work with only the coupled set. The rest of the analysis follows precisely as given in Lamb for these modified equations. We now specify disturbances on the first row by $\hat{x}_m = a_1 e^{im\phi}$, and $\hat{y}_m = b_1 e^{im\phi}$, and for disturbances on the second row by $\hat{x}_n = a_2 e^{in\phi}$, and $\hat{y}_n = b_2 e^{in\phi}$, where $-\pi \leqslant \phi \leqslant \pi$. The stability equations for the first row are

$$\frac{2\pi l^2}{\Gamma}\frac{da_1}{dt} = \qquad -(A-\eta)\,b_1 - Ba_2 - Cb_2, \tag{2.12a}$$

$$\frac{2\pi l^2}{\Gamma}\frac{db_1}{dt} = -(\tilde{A}+\eta)\,a_1 \qquad -\tilde{C}a_2 + \tilde{B}b_2, \tag{2.12b}$$

where $\eta = (kl)^2\theta(ka)$, and for the symmetric double row

$$A = \sum_p{}' \frac{1-\psi(|p|\,kl)\,e^{ip\phi}}{p^2} - \sum_q \frac{q^2-\kappa^2}{(q^2+\kappa^2)^2}$$

$$= \tfrac{1}{3}\pi^2 - 2\sum_{p=1}^{\infty} \frac{\psi(pkl)\cos p\phi}{p^2} + \frac{\pi^2}{\sinh^2\kappa\pi}, \tag{2.13}$$

$$B = \sum_q \frac{q\kappa}{(q^2+\kappa^2)^2}\left[\chi((q^2+\kappa^2)^{\frac{1}{2}}kl) + \psi((q^2+\kappa^2)^{\frac{1}{2}}kl)\right]e^{iq\phi}$$

$$= 2i\sum_{q=1}^{\infty} \frac{q\kappa}{(q^2+\kappa^2)^2}\left[\chi((q^2+\kappa^2)^{\frac{1}{2}}kl) + \psi((a^2+\kappa^2)^{\frac{1}{2}}kl)\right]\sin q\phi, \tag{2.14}$$

$$C = \sum_q \frac{q^2\psi((q^2+\kappa^2)^{\frac{1}{2}}kl) - \kappa^2\chi((q^2+\kappa^2)^{\frac{1}{2}}kl)}{(q^2+\kappa^2)^2}e^{iq\phi}$$

$$= -\frac{\chi(\kappa kl)}{\kappa^2} + 2\sum_{q=1}^{\infty} \frac{q^2\psi((q^2+\kappa^2)^{\frac{1}{2}}kl) - \kappa^2\chi((q^2+\kappa^2)^{\frac{1}{2}}kl)}{(q^2+\kappa^2)^2}\cos q\phi, \tag{2.15}$$

where $\kappa = h/l$ is the ratio of the distance h between the rows and the separation l of vortices on a single row. $\tilde{A}$, $\tilde{B}$, and $\tilde{C}$ are found by interchanging the symbols χ and ψ in the above equations.

The corresponding equations for the lower row are found by reversing the signs of Γ and κ and interchanging the subscripts 1 and 2. Thus

$$\frac{2\pi l^2}{\Gamma}\frac{da_2}{dt} = (A-\eta)\,b_2 - Ba_1 + Cb_1, \tag{2.16a}$$

$$\frac{2\pi l^2}{\Gamma}\frac{db_2}{dt} = (\tilde{A}+\eta)\,a_2 + \tilde{C}a_1 + \tilde{B}b_1. \tag{2.16b}$$

We now look at symmetric and antisymmetric modes with respect to a plane midway between the two parallel rows,

$$a_{\mathrm{S}} = a_1 + a_2, \quad b_{\mathrm{S}} = b_1 - b_2, \quad a_{\mathrm{A}} = a_1 - a_2, \quad b_{\mathrm{A}} = b_1 + b_2. \tag{2.17}$$

Introducing disturbances proportional to $e^{\sigma t}$, the eigenvalue problem reduces to

$$\hat{\sigma}_l a_{\mathrm{S}} = -Ba_{\mathrm{S}} - (A-C-\eta)\,b_{\mathrm{S}}, \tag{2.18a}$$

$$\hat{\sigma}_l b_{\mathrm{S}} = -(\tilde{A}+\tilde{C}+\eta)\,a_{\mathrm{S}} - \tilde{B}b_{\mathrm{S}}; \tag{2.18b}$$

$$\hat{\sigma}_l a_{\mathrm{A}} = +Ba_{\mathrm{A}} - (A+C-\eta)\,b_{\mathrm{A}}, \tag{2.18c}$$

$$\hat{\sigma}_l b_{\mathrm{A}} = -(\tilde{A}-\tilde{C}+\eta)\,a_{\mathrm{A}} + \tilde{B}b_{\mathrm{A}}; \tag{2.18d}$$

where $\hat{\sigma}_l = 2\pi l^2\sigma/\Gamma$ is the non-dimensional growth rate based on constant l and Γ. This transformation reduces the determination of linear stability or instability to a question of the character of roots of quadratic equations. Since $B = \tilde{B}$, the solution of the equations is especially simple so that we have

$$\hat{\sigma}_l^{\mathrm{S}} = -B \pm [(A-C-\eta)\,(\tilde{A}+\tilde{C}+\eta)]^{\frac{1}{2}}, \tag{2.19a}$$

$$\hat{\sigma}_l^{\mathrm{A}} = +B \pm [(A+C-\eta)\,(\tilde{A}-\tilde{C}+\eta)]^{\frac{1}{2}}. \tag{2.19b}$$

Since B is purely imaginary the stability of the configuration is determined only by the sign of the products in the square-root term. If the product is negative the system is neutrally stable, if positive the system is unstable.

The variable ϕ must be allowed to vary continuously in the range $-\pi \leqslant \phi \leqslant \pi$. However, since negative values of ϕ simply give the complex-conjugate eigenfunctions

of those with ϕ positive, it is sufficient to consider values of ϕ only in the range $0 \leqslant \phi \leqslant \pi$. Now ϕ/l may be thought of as the wavenumber of the disturbance in the row direction, so that $2\pi l/\phi = \mu l$ is the wavelength in the row direction with $2 \leqslant \mu \leqslant \infty$. Thus $\mu = 2{\cdot}0$ implies a repetition every two vortices, $\mu = 4{\cdot}0$ a repetition every four vortices, and $\mu = \infty$ implies that all the vortices on a single row when viewed in an (x, y)-plane cross-section are displaced in the same direction. It is important to realize that $\mu = \infty$ implies a simple translation of the whole row as a unit only for the case $kl = 0{\cdot}0$. That is, the magnitude and sign of the two-dimensional displacements in a given (x, y)-plane will vary with z for finite values of the axial wavelength λ.

In the symmetric mode $a_1 = a_2$ and $b_1 = -b_2$. This mode can therefore be thought of as a row of vortices near a wall with the second row representing an image system. In the antisymmetric mode $a_1 = -a_2$ and $b_1 = b_2$, so that one may visualize in a given (x, y)-plane each pair of vortices (separated by h in the y-direction) being displaced in opposite x-directions about their common (y, z)-plane but equally displaced in the y-direction.

The subscript l on $\hat{\sigma}_l^{\mathrm{S}}$ and $\hat{\sigma}_l^{\mathrm{A}}$ refers to the way σ is non-dimensionalized. A subscript l means we base σ on constant l and Γ. Changes in $\kappa = h/l$ then refer to changes in h alone. It is equally feasible to non-dimensionalize on h and Γ so that changes in κ refer to changes in l. In this case $\kappa = 0$ corresponds to an isolated pair of translating vortices. It is clear that $\hat{\sigma}_h = \kappa^2 \hat{\sigma}_l$, where in the computation of $\hat{\sigma}_l$ we replace kl by kh/κ.

We now pass easily to the case of the staggered double row of vortices or the Kármán vortex street. The disturbances on the first row are given by $\hat{x}_n = a_1 e^{im\phi}$, and $\hat{y}_m = b_1 e^{im\phi}$, and on the second row by $\hat{x}_n = a_2 e^{i(n+\frac{1}{2})\phi}$, and $\hat{y}_n = b_2 e^{i(n+\frac{1}{2})\phi}$, where $-\pi \leqslant \phi \leqslant \pi$. The corresponding stability equations are exactly the same if we replace q by $q+\frac{1}{2}$ in (2.13)–(2.15). Thus

$$A = \sum_p{}' \frac{1-\psi(|p|\,kl)\,e^{ip\phi}}{p^2} - \sum_q \frac{(q+\frac{1}{2})^2-\kappa^2}{((q+\frac{1}{2})^2+\kappa^2)^2}$$

$$= \tfrac{1}{3}\pi^2 - 2\sum_{p=1}^{\infty} \frac{\psi(pkl)\cos p\phi}{p^2} - \frac{\pi^2}{\cosh^2 \kappa\pi}, \tag{2.20}$$

$$B = \sum_q \frac{(q+\frac{1}{2})\,\kappa}{((q+\frac{1}{2})^2+\kappa^2)^2}[\chi(((q+\tfrac{1}{2})^2+\kappa^2)^{\frac{1}{2}} kl) + \psi(((q+\tfrac{1}{2})^2+\kappa^2)^{\frac{1}{2}} kl)]\, e^{i(q+\frac{1}{2})\phi}$$

$$= 2i\sum_{q=0}^{\infty} \frac{(q+\frac{1}{2})\,\kappa}{((q+\frac{1}{2})^2+\kappa^2)^2}[\chi(((q+\tfrac{1}{2})^2+\kappa^2)^{\frac{1}{2}} kl) + \psi(((q+\tfrac{1}{2})^2+\kappa^2)^{\frac{1}{2}} kl)]\sin(q+\tfrac{1}{2})\phi, \tag{2.21}$$

$$C = \sum_q \frac{(q+\frac{1}{2})^2\,\psi(((q+\frac{1}{2})^2+\kappa^2)^{\frac{1}{2}} kl) - \kappa^2\chi(((q+\frac{1}{2})^2+\kappa^2)^{\frac{1}{2}} kl)}{((q+\frac{1}{2})^2+\kappa^2)^2} e^{i(q+\frac{1}{2})\phi}$$

$$= 2\sum_{q=0}^{\infty} \frac{(q+\frac{1}{2})^2\,\psi(((q+\frac{1}{2})^2+\kappa^2)^{\frac{1}{2}} kl) - \kappa^2\chi(((q+\frac{1}{2})^2+\kappa^2)^{\frac{1}{2}} kl)}{((q+\frac{1}{2})^2+\kappa^2)^2} \cos(q+\tfrac{1}{2})\phi, \tag{2.22}$$

with $\tilde{A}$, $\tilde{B}$ and $\tilde{C}$ again found by interchanging the symbols ψ and χ. As before it is sufficient for stability considerations to consider ϕ in the range $0 \leqslant \phi \leqslant \pi$ or $2 \leqslant \mu \leqslant \infty$ for both the symmetric and antisymmetric modes. The geometrical meaning of each mode can be clarified by assuming a very long row-wise disturbance wavelength. The symmetric mode in any (x, y) cross-section would then appear only as a change in the y-dimension of the street without changing the relative row-wise

alignment of the street. The antisymmetric mode on the other hand would appear in the same section to cause a relative change in the spacing in the x-direction between vortices on the first and second rows of the street.

The case of the single row of vortices is easily obtained from the above by dropping all quantities relating to the second row. Thus

$$\frac{2\pi l^2}{\Gamma}\frac{da_1}{dt} = -(A-\eta)\,b_1, \tag{2.23a}$$

$$\frac{2\pi l^2}{\Gamma}\frac{db_1}{dt} = -(\tilde{A}+\eta)\,a_1, \tag{2.23b}$$

so that

$$\hat{\sigma}_l = \pm[(A-\eta)\,(\tilde{A}+\eta)]^{\frac{1}{2}}, \tag{2.24a}$$

$$A = \sum_p{}' \frac{1-\psi(|p|\,kl)\,e^{ip\phi}}{p^2} = \tfrac{1}{3}\pi^2 - 2\sum_{p=1}^{\infty}\frac{\psi(pkl)}{p^2}\cos p\phi. \tag{2.24b}$$

It is again sufficient to consider only the range $2 \leqslant \mu \leqslant \infty$ for considerations of stability.

Sections 3–6 will be devoted to a description of the stability diagrams computed from the above formula. When the growth rate is based on constant l it is convenient to introduce the notation $\alpha_l + i\beta_l = 2\hat{\sigma}_l/\pi^2$. Then α_l represents the real part of the eigenvalue with this growth rate non-dimensionalized on constant l and Γ. The factor $2/\pi^2$ normalizes the maximum growth rate of the single infinite row to the value 1. We define α_h in a similar manner to the real part of $\hat{\sigma}_h$.

3. Single row

The single infinite row of corotating vortices is, of course, always unstable to pure two-dimensional disturbances. The most unstable mode is the pairing instability whereby adjacent vortices are displaced in opposite directions. This mode corresponds to $\mu = 2{\cdot}0$. As $\mu \to \infty$, this maximum growth rate decreases to zero. Figure 2 shows that as $l/\lambda = kl/2\pi$ increases, the growth rates fall rapidly to zero. This is due to the self-induced straining field counteracting the induced strain of the other vortices. As l/λ increases, the functions χ and ψ fall quickly to zero, so that mutual-interaction effects are soon negligible and only the zeroth-order strain from the other vortices and the self-induced strain contribute to the stability equations. For small axial wavelengths, as the self-induced strain goes to zero, the vortex becomes unstable to the straining field of the other vortices in the row. Figure 2 is for $a/l = 0{\cdot}1$. This value of a/l was chosen in order to include the indication of the short-transverse-wavelength parametric instability in the diagram. We stress again that the instability shown is only representative of a phenomena that occurs only when the internal structure of the vortex allows. For smaller vortex area a much larger l/λ is required to obtain the value $ka = 1{\cdot}44$ that is the zero of the self-induction function. The effect of smaller a/l on the long-axial-wavelength instability is to decrease the width of the unstable region near $l/\lambda = 0$. No qualitative features are changed.

The stability diagrams shown are consistent with well-known observed behaviour in the mixing layer whereby vortices that form from the Kelvin–Helmholtz instability are observed to undergo a pairing interaction (Roshko 1976). It is seen in the stability diagrams that three-dimensional disturbances have a smaller growth rate than the pure two-dimensional pairing mode. This may in part account for the continued strong two-dimensional character of the mixing layer as it develops through a pairing process.

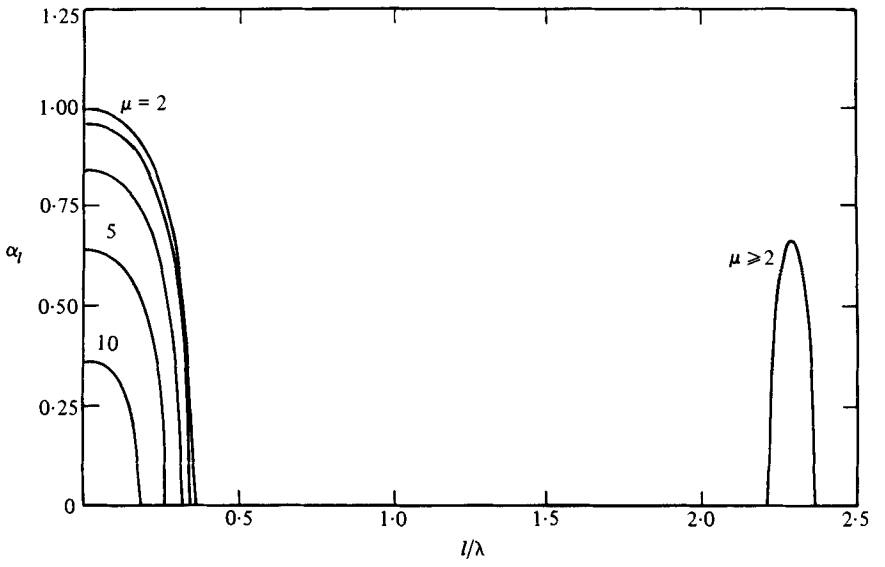

FIGURE 2. Plot of the growth rate α_l versus l/λ for various values of μ and $a/l = 0{\cdot}1$ in the case of the single row.

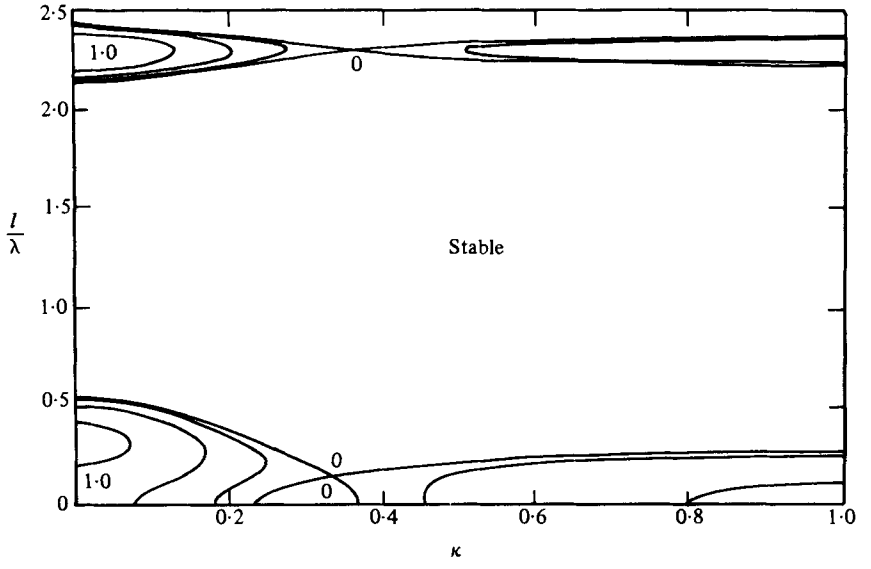

FIGURE 3. Contour plot of α_l^{A} in κ and l/λ for $\mu = 4{\cdot}0$ and $a/l = 0{\cdot}1$ in the case of the staggered double row.

4. Staggered double row or Kármán vortex street

The staggered double row of vortices that appears in the wake of many different objects over a wide range of Reynolds numbers has long been an enigma to both theoreticians and experimenters alike. Kármán, in his original papers, predicted two values of the spacing ratio for the staggered vortex street. In his first paper he allowed perturbations to only a pair of vortices. The value of the street spacing ratio then

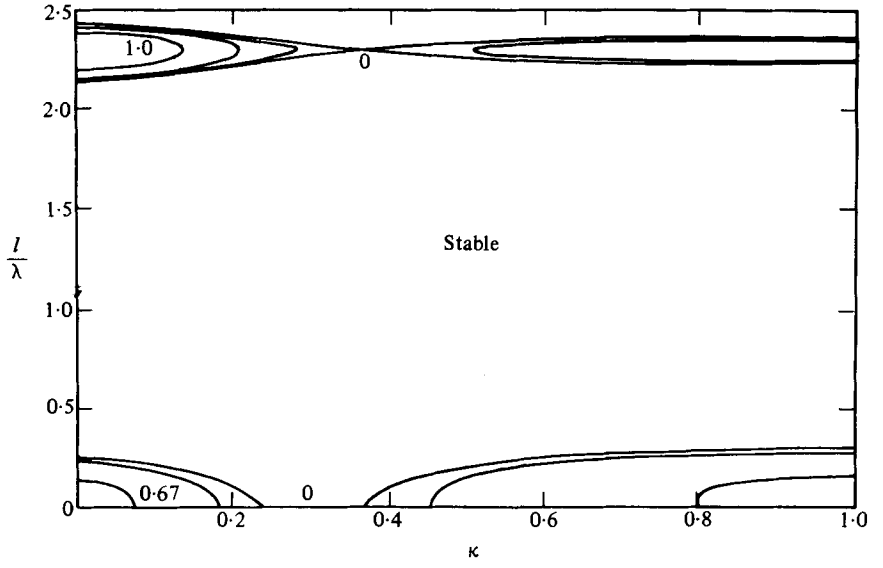

FIGURE 4. Contour plot of α_l^S in κ and l/λ for $\mu = 4{\cdot}0$ and $a/l = 0{\cdot}1$ in the case of the staggered double row.

obtained by requiring neutral stability to infinitesimal two-dimensional disturbances was $\cosh \kappa\pi = \sqrt{3}$ or $\kappa = 0{\cdot}365$. In subsequent papers, by allowing two-dimensional perturbations to all of the vortices in the two rows the value of $\cosh \kappa\pi = \sqrt{2}$ or $\kappa = 0{\cdot}281$ was obtained. Both of these values will appear in the subsequent investigation. It is now known of course that the street is unstable to two-dimensional finite-amplitude disturbances (Schmieden 1936; Kochin 1939; Domm 1956). Indeed there are questions about the relevance of the stability calculations to the appearance of the street at all (Saffman & Schatzman 1982*b*).

Upon introducing disturbances in the spanwise or axial direction one finds the stability characteristics to depend significantly on the axial wavelength. Figures 3 and 4 give important features of the stability diagrams for the antisymmetric and symmetric modes, respectively. These figures are for $\mu = 4{\cdot}0$. In figure 3 a long-axial-wavelength instability is always observed at some value of l/λ even though a pure two-dimensional mode may be stable. The neutrally stable saddle point moves down to the κ-axis as $\mu \to 2{\cdot}0$, and the small region of stability below the saddle point disappears. The saddle point lies at a value $\kappa = 0{\cdot}281$ when $\mu = 2{\cdot}0$. For larger values of μ the saddle point moves toward the lower right-hand corner of the diagram and the growth rates to the right of the saddle decrease to zero. On the other hand, as $\mu \to \infty$, even though strictly two-dimensional modes become neutrally stable, the large growth rates for three-dimensional modes to the left of the saddle point increase in magnitude.

The symmetric mode exhibits much-simpler characteristics. Figure 4 shows the growth-rate curves for $\mu = 4{\cdot}0$. Note the region of neutral stability to long-wavelength axial disturbances. For $\mu \to 2{\cdot}0$ this region decreases to a single point $\kappa = 0{\cdot}281$. As $\mu \to \infty$ the stable region grows until for $\mu = \infty$ all long-wavelength axial modes are stable.

In figure 5 we plot the maximum over l/λ and μ of the growth rates as well as the

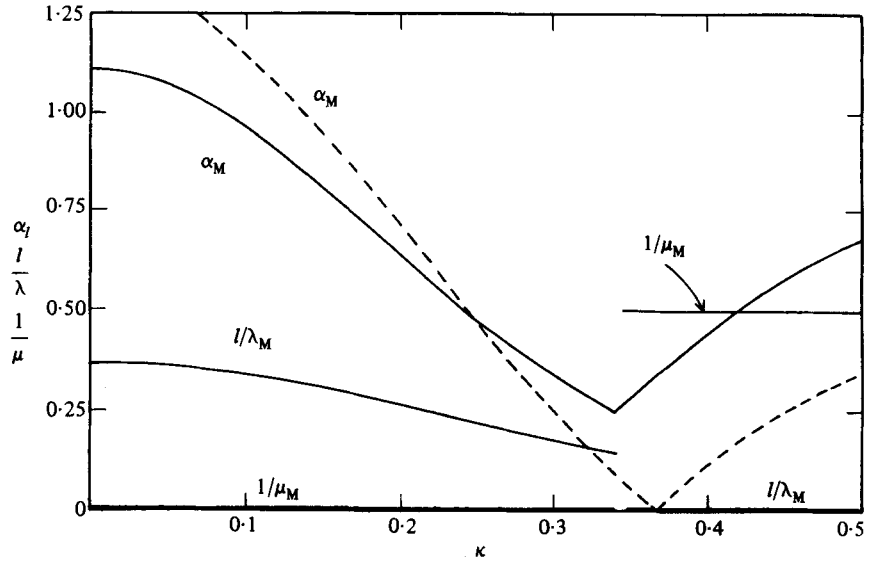

FIGURE 5. Plot of the maximum growth rate α_l^A and the corresponding l/λ and $1/\mu$, all versus κ for $a/l = 0{\cdot}1$ in the case of the staggered double row. Also plotted is the short-axial-wavelength growth rate (dashed curve). Subscript M denotes maximum.

values of these parameters at which the maximum occurs. The maximum growth rate occurs for the antisymmetric mode and $\mu = \infty$ for κ less than a value between 0·3 and 0·4. For larger values of κ the dominant instability is a two-dimensional mode with $\mu = 2{\cdot}0$. The precise value of κ at which the characteristics of the dominant mode change is dependent on a/l and increases slightly with decreasing a/l.

As l/λ increases, the functions χ and ψ rapidly approach zero, so that the effect of the displacement of the other vortices has little to do with the stability of the given vortex filament. The growth rate then becomes essentially a function of κ and the self-induction function. At a value of l/λ such that the parametric instability is possible the magnitude of this instability is a function of κ. The point of zero growth rate, as can be seen from (2.20) and (2.22), approaches the value of κ given by $\cosh \kappa\pi = \sqrt{3}$ for large l/λ. This is essentially the value of the spacing ratio at which the straining field due only to the zeroth-order fields of the other vortices is negligible. As mentioned before, this is the value of the spacing ratio first proposed by Kármán (1911). This is also the value at which two-dimensional vortices of small size change from being elongated in the transverse direction to being longer in the streamwise direction (Saffman & Schatzman 1981). The growth rate for the short-wavelength instability, computed by neglecting exponentially small terms in l/λ, is shown by the dotted line in figure 5.

As in the case of the single row, smaller values of a/l have the effect of decreasing the width in l/λ of the unstable region near $l/\lambda = 0$, and also of increasing the magnitude of the $\mu = \infty$ growth rate. The short-wavelength instabilities also occur at correspondingly larger values of l/λ. It is interesting to note that both long- and short-axial-wavelength modes have maximum growth rates that are smallest for values of κ from about 0·3 to 0·4. For κ less than about 0·3, the dominant long-wavelength axial mode is a three-dimensional mode with $\mu = \infty$. Whether this mode or the short-wavelength mode has a larger growth rate depends on the precise

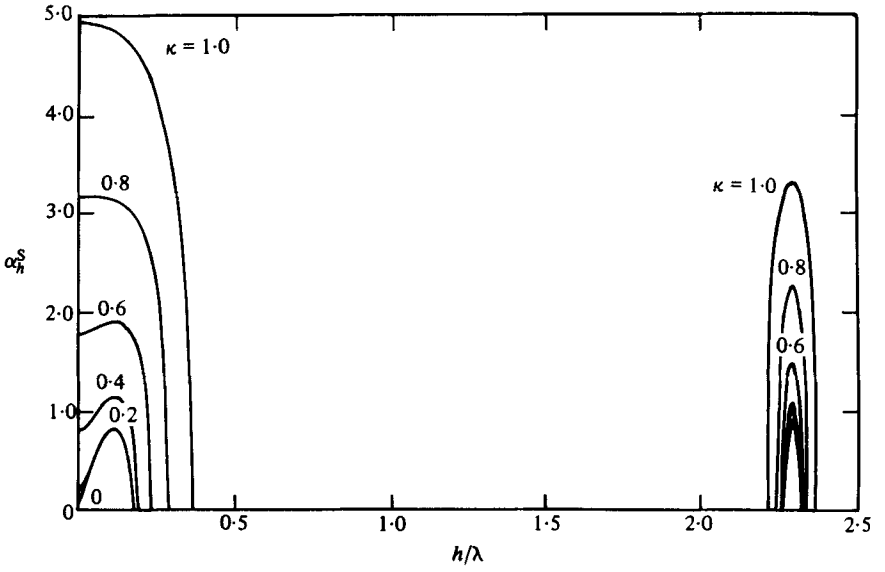

FIGURE 6. Plot of α_h^S versus h/λ for various values of κ with $\mu = 2{\cdot}0$ and $a/h = 0{\cdot}1$ in the case of the symmetric double row.

value of a/l. For very small a/l the long-wavelength mode is dominant. When κ is greater than about 0·4, the two-dimensional $\mu = 2{\cdot}0$ instability is dominant.

The effect of significant vortex area has an as yet undetermined effect on the three-dimensional stability of the vortex street. As mentioned earlier, larger vortex area will stabilize the street to two-dimensional disturbances for a small interval about $\kappa = 0{\cdot}281$. Whether significant finite area will reduce and/or eliminate the instability for a three-dimensional disturbance is unknown but seems possible. There is no doubt however that the third dimension is of great importance in discussing the stability of the Kármán vortex street and must be a part of any consistent theory for its existence and evolution.

5. Symmetric vortex street

It is instructive to view the case of the symmetric vortex street in terms of constant h. Thus changes in κ refer to changes in l and we now plot $\mathrm{Re}\,\hat{\sigma}_h = \alpha_h$. For $\kappa = 0{\cdot}0$ we find the results of Gopal and Crow for a pair of corotating line vortices. Figure 6 gives growth rate diagrams for the symmetric mode. It is observed that for long axial wavelengths the configuration is always unstable. For values of κ less than one, the most unstable mode has a finite wavelength in the axial direction. For larger κ, a pure two-dimensional mode is most unstable. It is seen that the most-unstable modes are at $\mu = 2{\cdot}0$, i.e. the pairing mode. As κ increases the magnitude of the growth rate also grows as the induced velocity of more vortices becomes effective. However, for μ near ∞ the growth rate no longer increases but rather decreases with increasing κ as seen in figure 7. For short axial wavelengths, no corresponding region of relatively small growth rate such as in the case of the Kármán vortex street is found. This is easily seen from the stability equations for large kl.

For the antisymmetric mode, figure 8 shows that the most-unstable configuration

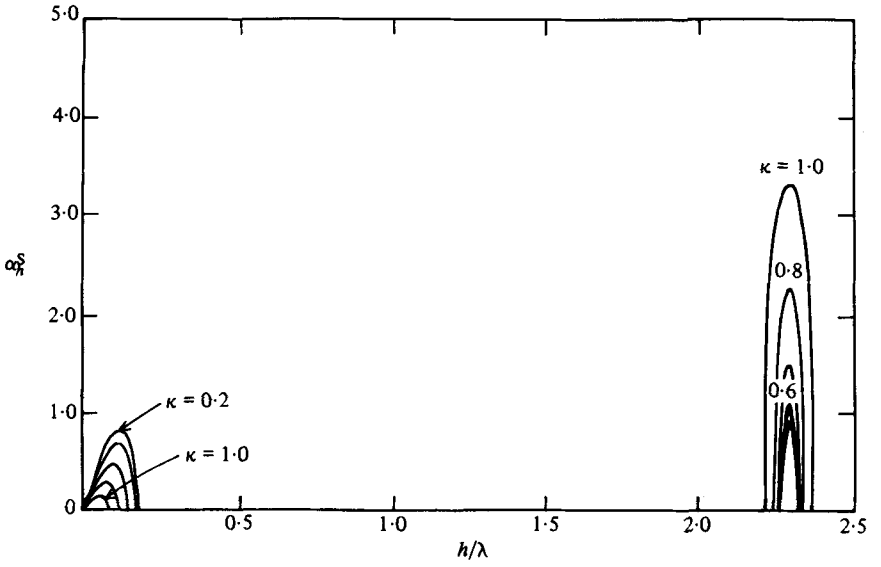

FIGURE 7. Plot of α_h^S versus h/λ for various values of κ with $\mu = \infty$ and $a/h = 0{\cdot}1$ in the case of the symmetric double row.

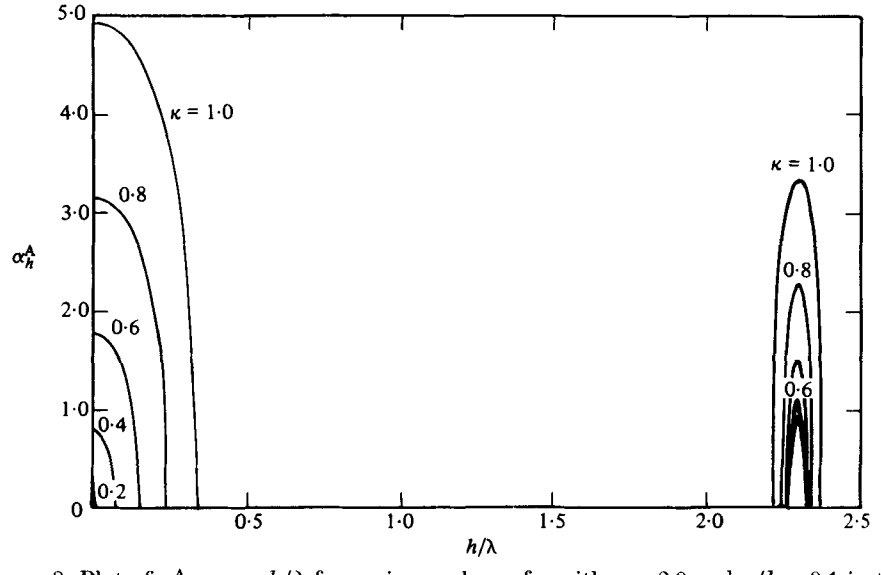

FIGURE 8. Plot of α_h^A versus h/λ for various values of κ with $\mu = 2{\cdot}0$ and $a/h = 0{\cdot}1$ in the case of the symmetric double row.

is always the two-dimensional pairing mode for long axial wavelengths. Larger μ only serves to decrease the growth rates until for $\mu = \infty$ the instability is reduced to zero for any value of κ. The short-axial-wavelength instability has the same characteristics as the symmetric mode.

Figure 9 gives the growth rates for the symmetric mode if we base the growth rate on l instead of h. In this case we cannot allow κ to become too small as the growth

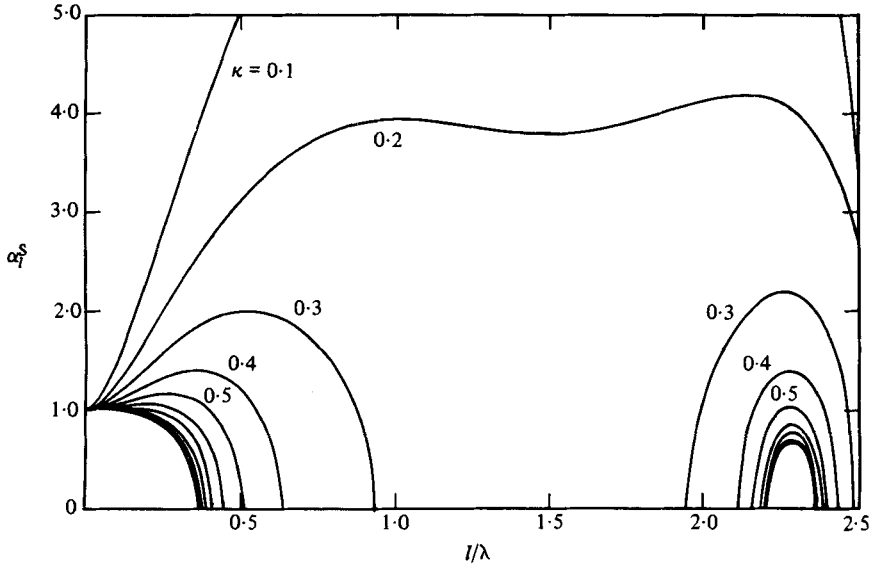

FIGURE 9. Plot of α_l^S versus l/λ for various values of κ with $\mu = 2{\cdot}0$ and $a/l = 0{\cdot}1$ in the case of the symmetric double row.

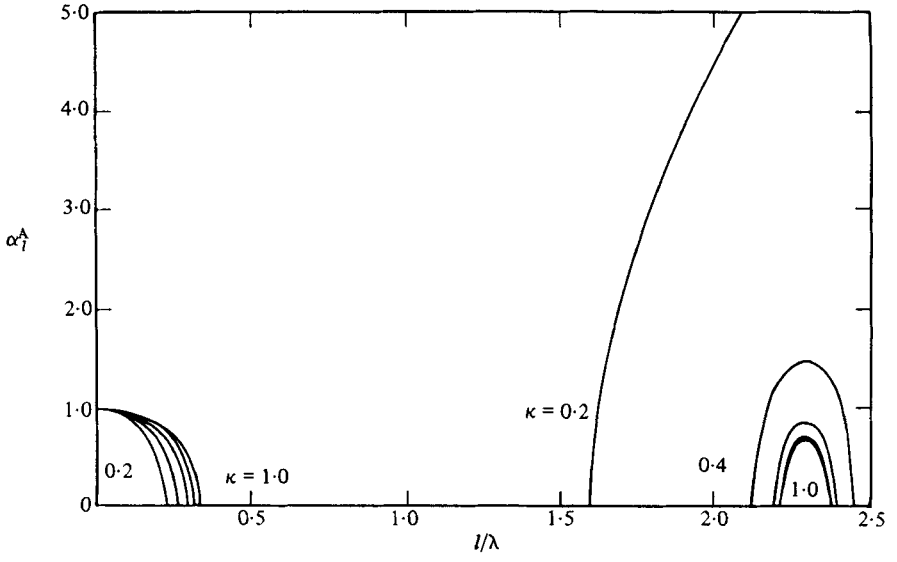

FIGURE 10. Plot of α_l^A versus l/λ for various values of κ with $\mu = 2{\cdot}0$ and $a/l = 0{\cdot}1$ in the case of the symmetric double row.

rates are based on l and become infinite as h/l goes to zero. The three-dimensional $\mu = 2{\cdot}0$ mode is most unstable. It is only for larger values of κ that the dominant instability approaches a pure two-dimensional mode. Increasing the wavelength in the row direction serves only to decrease the magnitude of the growth rate, and in general, except for very long axial wavelengths, this decrease is slight.

For the antisymmetric mode, figure 10 indicates that the long-axial-wavelength instability is present but not as strong as the symmetric-mode instability. It is seen

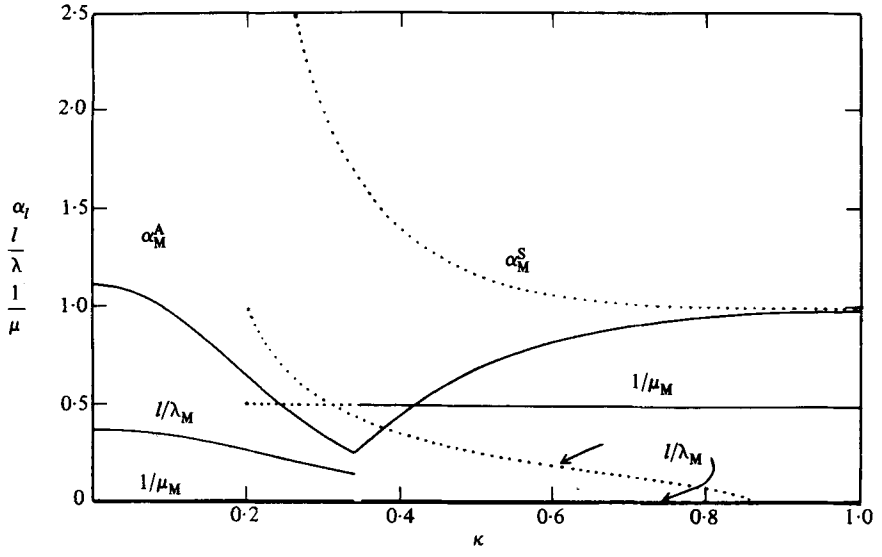

FIGURE 11. Plot of maximum α_l^A for the staggered double row and maximum α_l^S for the symmetric double row versus κ for $a/l = 0{\cdot}1$. Maximum is over long-axial-wavelength region only. Also plotted are the values of l/λ and $1/\mu$ at which the maximum occurs. Solid lines refer to the staggered double row and dotted lines to the symmetric double row. Subscript M denotes maximum.

that a change in κ has a minor effect and that the characteristics of the long-axial-wavelength instability are very much like the single vortex row. The dominant growth rate is for a two-dimensional, pairing instability.

For both the symmetric and antisymmetric modes the short-axial-wavelength instability is always present and the growth rate increases monotonically with decreasing κ. In the case of the symmetric mode for $a/l = 0{\cdot}1$ and κ small, the long- and short-axial-wavelength growth-rate curves merge to give a bimodal curve such as seen in figure 9.

The symmetric mode models the effect of a wall on a single row of vortices as the second row represents an image system of vortices. It is clear from the figures that the symmetric mode is always unstable. Not only are two-dimensional disturbances unstable, but in general, for a given κ, there is a three-dimensional disturbance that has a larger growth rate. Moreover, the row-wise wavelength for the maximum instability is the $\mu = 2{\cdot}0$ or pairing-type instability. This suggests that, provided a real flow may be modelled initially by a system of vortices of the type considered, one would expect a strong three-dimensional instability to develop.

6. Relative instability of the configurations

It is now of interest to compare the magnitudes of the maximum growth rates for the three different configurations over various values of κ for the long-wavelength instability. We consider only the symmetric mode for the symmetric double row, but both the symmetric and antisymmetric mode for the staggered double row. In the case of the staggered double row the maximum always occurs for the antisymmetric mode although when $\mu = 2{\cdot}0$ this maximum is also attained for the symmetric mode.

Figure 11 shows the maximum growth rates for the staggered and symmetric

double rows, as well as the values of l/λ and $1/\mu$ at which the maxima occur. The single row corresponds to the $\kappa \to \infty$ limit, and we see that the $\mu = 2{\cdot}0$, two-dimensional, pairing instability is the dominant instability. The most obvious feature of the graphs is that the growth rate of the symmetric double row is always the largest of the three, while except for a region near $\kappa = 0$ the staggered double row has the smallest growth rate. The symmetric double row is most unstable always for the $\mu = 2{\cdot}0$ mode, with the corresponding value of λ decreasing with decreasing κ. On the other hand, the staggered double row is most unstable at the values $\mu = 2{\cdot}0$ and $l/\lambda = 0$ for all κ greater than about 0·3–0·4. For smaller values of κ the most-unstable mode switches to a $\mu = \infty$ mode with l/λ of the maximum increasing slightly as κ decreases.

The dependence of the diagram on a/l is very weak. A smaller value of a/l has the effect of increasing the magnitude of the three-dimensional mode for the staggered double row as well as the value of κ at which the two-dimensional mode becomes dominant. The value of l/λ for a dominant three-dimensional mode decreases with decreasing a/l for both array configurations.

These results indicate that the fastest-growing symmetric disturbances to the symmetric double row, which is a model for the boundary layer, are three-dimensional, and have larger growth rates than those of the staggered double row and the single row. These configurations are models for the wake and the mixing layer respectively. The mixing-layer model indicates maximum instability for a two-dimensional pairing mode. The wake model, on the other hand, indicates that the wake is most unstable to a three-dimensional disturbance for small values of the street spacing ratio, while for larger values of the spacing ratio a two-dimensional pairing mode is most unstable. The third dimension is thus seen to be a significant factor in discussing the stability of configurations of finite-area vortices and ought not to be neglected when discussing the stability of real two-dimensional flows that may be modelled by inviscid vortex filaments.

This work was supported by NASA Lewis Research Center (NAG 3-179) and the Department of Energy (Office of Basic Energy Sciences).

REFERENCES

Christiansen, J. P. & Zabusky, N. J. 1973 Instability, coalescence and fission of finite-area vortex structures. *J. Fluid Mech.* **61**, 219–243.

Crow, S. C. 1970 Stability theory for a pair of trailing vortices. *A.I.A.A. J.* **8**, 2172–2179.

Domm, U. 1956 Über die Wirbelstraßen von geringster Instabilität. *Z. angew. Math. Mech.* **36**, 367–371.

Gopal, E. S. R. 1963 Motion and stability of quantized vortices in a finite channel: Application to liquid helium II. *Ann. Phys. (N.Y.)* **25**, 196–220.

Jimenez, J. 1975 Stability of a pair of co-rotating vortices. *Phys. Fluids* **18**, 1580–1581.

Kármán, T. von 1911 Über den Mechanismus des Widerstands, den ein bewegter Körper in einer Flüssigkeit erfährt. *Göttinger Nachrichten, Math. Phys. Kl.*, 509–517.

Kármán, T. von 1912 Über den Mechanismus des Widerstands, den ein bewegter Körper in einer Flüssigkeit erfährt. *Göttinger Nachrichten, Math. Phys. Kl.*, 547–556.

Kármán, T. von & Rubach, H. L. 1912 Über den Mechanismus des Flüssigkeits- und Luftwiderstands. *Phys. Z.* **13**, 49–59.

Kochin, N. J. 1939 On the instability of von Kármán's vortex street. *Dokl. Akad. Nauk SSSR* **24**, 19–23.

LAMB, H. 1932 *Hydrodynamics.* Cambridge University Press.

MOORE, D. W. & SAFFMAN, P. G. 1972 The motion of a vortex filament with axial flow. *Phil. Trans. R. Soc. Lond.* A **272**, 403–429.

MOORE, D. W. & SAFFMAN, P. G. 1974 A note on the stability of a vortex ring of small cross-section. *Proc. R. Soc. Lond.* A **338**, 535–537.

MOORE, D. W. & SAFFMAN, P. G. 1975 The instability of a straight vortex filament in a strain field. *Proc. R. Soc. Lond.* A **346**, 413–425.

PIERREHUMBERT, R. T. 1980 The structure and stability of large vortices in an inviscid flow. *M.I.T. Fluid Dynamics Lab. Rep.* no. 80–1.

PIERREHUMBERT, R. T. & WIDNALL, S. E. 1982 The two- and three-dimensional instabilities of a spatially periodic shear layer. *J. Fluid Mech.* **114**, 59–82.

ROSENHEAD, L. 1930 The spread of vorticity in the wake behind a cylinder. *Proc. R. Soc. Lond.* A **127**, 590–612.

ROSENHEAD, L. 1953 Vortex systems in wakes. *Adv. Appl. Mech.* **3**, 185–195.

ROSHKO, A. 1976 Structure of turbulent shear flows: A new look. *A.I.A.A. J.* **14**, 1349–1357.

SAFFMAN, P. G. 1981 Dynamics of vorticity. *J. Fluid Mech.* **106**, 49–58.

SAFFMAN, P. G. & BAKER, G. R. 1979 Vortex interactions. *Ann. Rev. Fluid Mech.* **11**, 95–122.

SAFFMAN, P. G. & SCHATZMAN, J. C. 1981 Properties of a vortex street of finite vortices. *SIAM J. Sci. Stat. Comp.* **2**, 285–295.

SAFFMAN, P. G. & SCHATZMAN, J. C. 1982*a* Stability of a vortex street of finite vortices. *J. Fluid Mech.* **117**, 171–185.

SAFFMAN, P. G. & SCHATZMAN, J. C. 1982*b* An inviscid model for the vortex-street wake. *J. Fluid Mech.* **122**, 467–486.

SAFFMAN, P. G. & SZETO, R. 1981 Structure of a linear array of uniform vortices. *Stud. Appl. Math.* **65**, 223–248.

SCHLAYER, K. 1928 Über die Stabilität der Kármánschen Wirbelstraße gegenüber beliebigen Störungen in drei Dimensionen. *Z. angew. Math. Mech.* **8**, 352–372.

SCHMIEDEN, C. 1936 Zur Theorie der Kármánschen Wirbelstraße. *Ing. Arch.* **7**, 215–221.

STUART, J. T. 1967 On finite amplitude oscillations in laminar mixing layers. *J. Fluid Mech.* **29**, 417–440.

WIDNALL, S. E. 1975 The structure and dynamics of vortex filaments. *Ann. Rev. Fluid Mech.* **7**, 141–165.

WIDNALL, S. E., BLISS, D. B. & TSAI, C-Y. 1974 The instability of short waves on a vortex ring. *J. Fluid Mech.* **66**, 35–47.

WILLE, R. 1960 Kármán vortex streets. *Adv. Appl. Mech.* **6**, 273–287.